FABRICATION AND PHOTOCATALYTIC ACTIVITY OF TiO$_2$ NANOTUBES BY HYDROTHERMAL TREATMENT

Y. SUN[a] , S. XU[b], J. Y. ZENG[c], S. S. YANG[a] , Q. R. ZHAO[a], Y. YANG[a], Q. ZHAO[b], G. X. WANG[b,*]
[a]*School of Mechanical Engineering, Chengdu University, Chengdu, 610106, China*
[b]*School of Chemical Engineering, Sichuan University, Chengdu, 610065, China*
[c]*School of Materials Science and Engineering, Southwest Jiaotong University, Chengdu, 610031, China*

TiO$_2$ nanotubes were prepared by hydrothermal method using P25 as raw material. The effect of hydrothermal duration and calcination temperature on the crystal structure and morphology of intermediate product and TiO$_2$ was investigated by XRD, SEM and TEM. The photocatalytic activity of TiO$_2$ was evaluated by the degradation of methylene blue. The result revealed the formation process of nanotube and indicated that the photocatalytic activity of TiO$_2$ nanotubes strongly depended on the calcination temperature. The crystallinity of nano-TiO$_2$ was gradually improved with the increasing calcination temperature up to 750 $^{\circ}$C resulting in the increase of degradation rate of methylene blue. With further increase in calcination temperature, anatase TiO$_2$ began to transform into rutile phase and the nanotubes completely transformed to particles, leading to the decrease of photocatalytic activity. It was found that TiO$_2$ annealed at 750 $^{\circ}$C showed the highest degradation rate, resulting from the excellent crystallinity of anatase phase and nanorod structure.

1. Introduction

Recently, TiO$_2$ has attracted much attention due to its unique properties and potential applications in photocatalysis, gas sensor, solar cells and lithium-ion batteries [1-4]. However, conventional TiO$_2$ powder photocatalyst with a low specific surface area limits the adsorption of pollutants on the surface of photocatalyst [5], which could lead to low photocatalytic efficiency. Therefore, to enhance photocatalytic activity, the synthesis of TiO$_2$ with one-dimensional structure has been developed by various methods, such as electrochemical anodization, hydrothermal treatment and template method [6-8]. Among these methods, hydrothermal route has been regarded as a relative facile technique to synthesize one-dimensional TiO$_2$, which can use TiO$_2$ powder, Ti powder, Ti foil and titanium alkoxides as source materials under alkaline, acidic and neutral conditions [9-12]. Moreover, the crystal structure, morphology and grain size of TiO$_2$ can be easily controlled by adjusting hydrothermal temperature, hydrothermal reaction time, reactant amount, pH of the solution and calcination temperature [13-17]. TiO$_2$ nanotubes (TNTs), a typical one-dimensional nanostructure material, have high surface area and the tubular structure may provide efficient route for charge transfer [18, 19], which are beneficial to improve the photocatalytic activity. Based on low-cost commercial Degussa P25, TiO$_2$ nanotubes can be synthesized by hydrothermal method with concentrated NaOH [20, 21]. Although many

---

* Corresponding author: guixin66@scu.edu.cn

investigations have been carried out for preparing TiO_2 nanotubes, the growth mechanism and process of TiO_2 nanotubes are still ambiguous because the hydrothermal reaction is a complicated process under high temperature and high pressure conditions. Hence it is necessary to further study the effect of hydrothermal parameters on the crystal structure and morphology of TiO_2 nanotubes. In this work, TiO_2 nanotubes have been prepared by hydrothermal method using P25 as raw material. In order to explore the growth process of nanotubes, the hydrothermal reaction time has been varied to observe the morphology change during hydrothermal process. To our best knowledge, there were few reports on the detailed changes in the morphology of the product in the hydrothermal reaction. Furthermore, the influence of calcination temperature on the crystallization, phase structure, morphology and photocatalytic activity evaluated by photocatalytic degradation of methylene blue (MB) dye has been investigated systematacially.

2. Experimental

TiO_2 nanotubes were prepared by hydrothermal method using TiO_2 (Degussa P25) powder as precursor. All of the chemical reagents used in the experiments were of analytical grade and without further purification. In a typical synthesis, 0.25 g of P25 powder was added in 30 mL of 10 M NaOH aqueous solution, followed by magnetic stirring. Then the mixture was transferred into a 50 mL Teflon-lined autoclave and heated at 180 ºC for different hydrothermal durations. After hydrothermal treatment, the products were washed with 0.1 M HCl solution and deionized water for several times until the pH value reached 7, and then dried in an oven at 80 °C. The TiO_2 nanotubes were obtained by calcining in the muffle furnace with various temperatures ranging from 450 ºC to 950 ºC for 2 h. The TNT samples were designed as TNT-450, TNT-550, TNT-650, TNT-750, TNT-850, TNT-950, respectively.

The crystal structure of samples was characterized by X-ray diffraction (XRD, DX 2700B, Dandong) with Cu Kα radiation. The morphologies of TNTs were observed by field-emission scanning electron microscopy (FESEM, Quanta 450, FEI) and high-resolution transmission electron microscope (HRTEM, JEM 2100F, Jeol).

The photocatalytic activity of TNTs was evaluated by the degradation of methylene blue (MB) under the irradiation of a 350 W xenon lamp (Solar-350, Beijing Nbet). Before irradiation, 0.1 g of TNTs were dispersed in 100 mL of MB solution (10 mg/L) and stirred for 30 min in the dark to reach adsorption-desorption equilibrium. The change in concentration of MB was measured by the UV-Vis spectrophotometer (UV-6100A, Shanghai Metash).

3. Results and discussion

3.1. Effect of hydrothermal duration

To explore the crystal structure change during the formation of TiO_2 nanotubes, hydrothermal treatment was carried out for different durations. After washing by HCl solution and deionized water, the intermediate products were obtained without calcination. As shown in Figure 1, the peaks of samples at 24.7° and 48.6° are assigned to $H_2Ti_4O_9 \cdot H_2O$ (JCPDS No. 36-0655). It is noted that with increasing hydrothermal reaction time, the crystallinity of hydrogen titanate samples was improved.
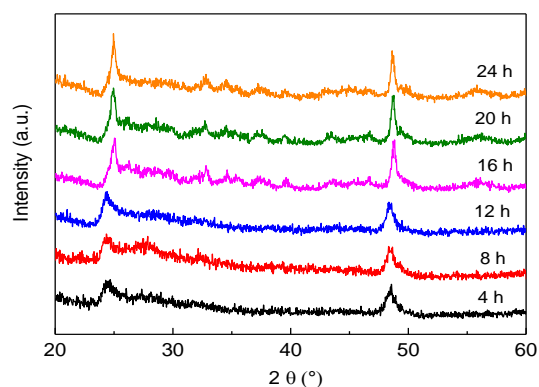
Fig. 1. XRD patterns of products before calcination obtained by different hydrothermal reaction times.

Based on the previous report [22], TiO_2 powders were dissolved in concentrated NaOH solution during the hydrothermal reaction and sodium titanate nanotubes were obtained. After acid washing, Na^+ ions were exchanged by H^+ ions, resulting in the intermediate products $H_2Ti_4O_9 \cdot H_2O$. After annealing, hydrogen titanate nanotubes can be transformed to TiO_2 and the result will be discussed in Fig. 3.
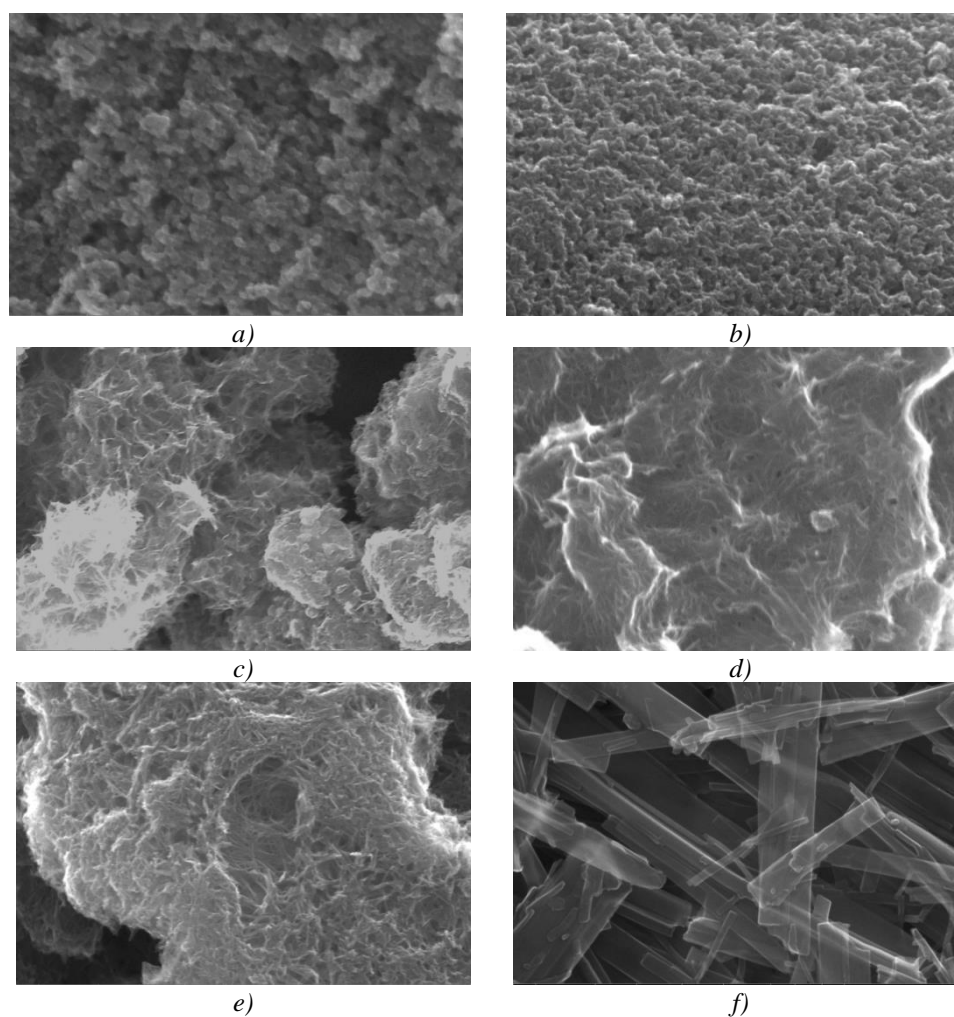

Fig. 2. SEM images of intermediate products with various hydrothermal durations: (a) 10 min, (b) 15 min, (c) 25 min, (d) 2 h, (e) 4 h and (f) 16 h.

Fig. 2 shows the effect of hydrothermal reaction time on the morphology of the intermediate products without calcination. In the initial stage of the hydrothermal process (Fig. 2 a-b), the product is still in the form of nanoparticles and the diameters of the nanoparticles are close to the starting material P25. After hydrothermal treatment of P25 for 25 minutes (Fig. 2 c), a nano-network structure is observed. With increasing hydrothermal reaction time (Fig. 2 d), nanotubes structure has formed and the diameters of the nanotubes are about 25 nm. As the reaction time reaches 4 h (Fig. 2 e), more nanotubes with the length of several micrometers are obtained. When the hydrothermal duration increases to 16 h, individual nanotubes with the diameter of around 100 nm are observed in Fig. 2 (f). This result reveals the formation process of nanotubes. Up to now, the formation mechanism of TiO_2 nanotubes prepared by hydrothermal method is still ambiguous. It is the most acceptable mechanism that TiO_2 nanoparticles are dissolved under alkaline circumstance and then form layered structure which could roll up into nanotubular structure [23]. However, there is no layered structure that can be seen in this study and most research.

3.2. Effect of calcination temperature

Fig. 3 shows the XRD patterns of TiO_2 nanotubes prepared by hydrothermal treatment of 24 h and calcined at different temperatures for 2 h. It can be seen clearly that the crystallinity of TiO_2 is poor at lower calcination temperature (450 °C and 550°C) and the weak peaks are indexed to monoclinic TiO_2 (B) phase (JCPDS No. 46-1237), which is consistent with previous report [24]. This result further confirms that P25 nanoparticles have been completely dissolved and form a new phase during the hydrothermal process. With increasing calcination temperature, the diffraction peaks become sharp and strong, indicating that the crystallinity of TiO2 is improved significantly.
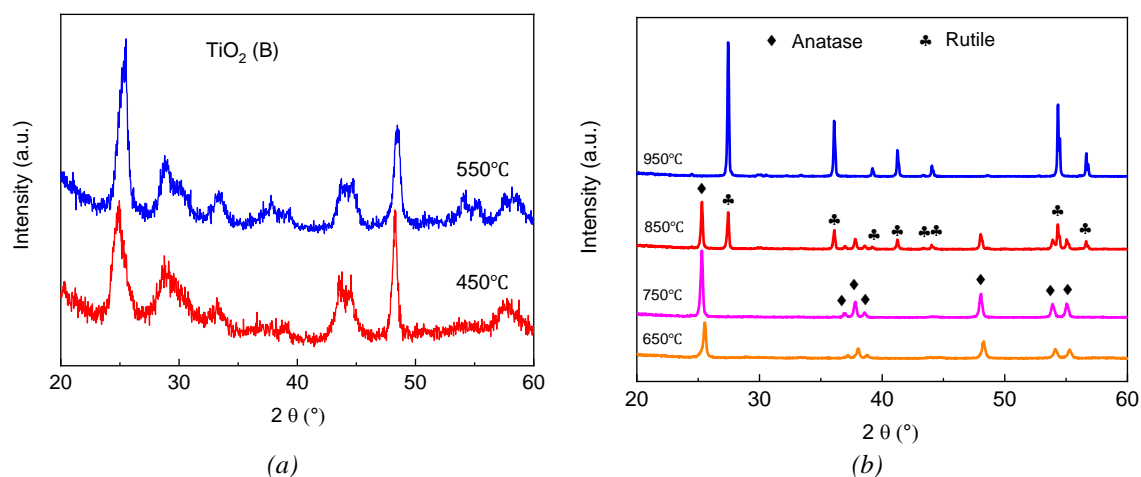

Fig. 3. XRD patterns of TiO_2 samples with different calcination temperatures.

The peaks at 25.3°, 37.0°, 37.8°, 38.6°, 48.1°, 53.9° and 55.0° are assigned to anatase phase (JCPDS No. 21-1272). It is noted that TiO_2 still exists in the form of anatase phase after calcination at 750°C, which is not in good agreement with most previous literatures [25, 26] that anatase TiO_2 can transform to rutile phase when the calcination temperature is higher than 550°C. This phenomenon can be explained that after dissolution and recrystallization during the hydrothermal process, the phase transition temperature of TiO_2 has been changed. At a higher temperature of 850°C, the peaks at 27.4°, 36.1°, 39.2°, 41.2°, 44.1°, 54.3°and 56.7° corresponding to rutile phase (JCPDS No. 6 5-0190) are observed, resulting in a hybrid structure of anatase and rutile phase. With further increase in the calcination temperature to 950°C, the anatase peaks are almost disappeared and only rutile diffraction peaks can be observed. The calculated result of average crystallite sizes and relative amounts of anatase and rutile are listed in Table 1. It is found that the average crystallite size of anatase and rutile phase both increase with increasing calcination temperature, which is attributed to the fact that higher annealing temperature has a

stimulative influence on grain growth. Comparing with the raw material P25, the relative mass fraction of anatase and rutile phase has a great change after hydrothermal treatment. When the annealing temperature increases to 750°C, only pure anatase phase can be obtained. With further increase in temperature (850°C), nearly 49.6% anatase TiO_2 has transformed to rutile phase. At 950°C, anatase phase has completely transformed to rutile phase.

Table 1. Average crystallite size and phase composition of TiO₂ nanotubes.

calcination temperature (°C)	average crystallite size (nm)		mass fraction (%)	
	anatase (101)	rutile (110)	anatase	rutile
P25	20.8	34.4	83.2	16.8
650	30.6	—	100	0
750	36.7	—	100	0
850	47.9	47.6	50.4	49.6
950	—	55.0	0	100

The surface morphology of TiO_2 nanotubes calcined at various temperatures is presented in Fig. 4. After hydrothermal process for 24 h, TiO_2 nanotubes structure can be seen clearly as the calcination temperature does not exceed 550°C (Fig. 4 a-b). With increasing annealing temperature to 650°C, TiO_2 nanoparticles are appeared accompanying with the decrease of nanotubes structure. When the annealing temperature is up to 750°C, the nanotubular structure has transformed to TiO_2 nanorod and the length of TiO_2 is decreased significantly. At higher calcination temperature above 850°C, the tubular structure has almost collapsed and all nanotubes have transformed to TiO_2 particles of half-micron size.
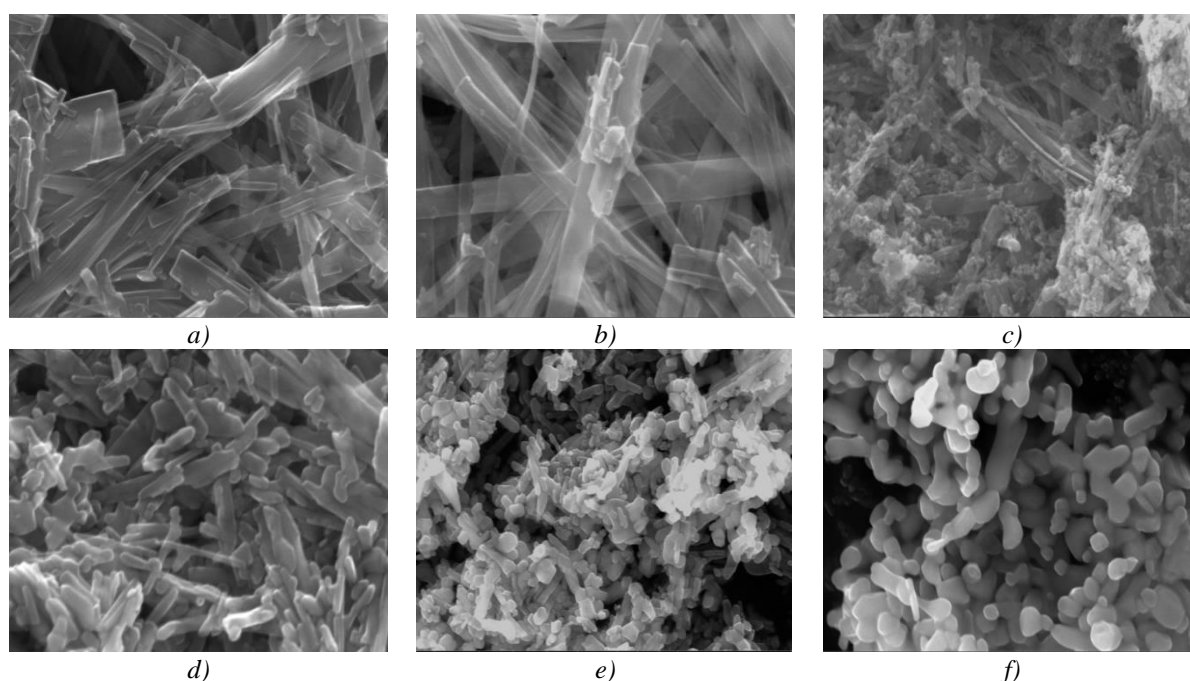

Fig. 4. SEM images of synthesized TiO₂ samples with various calcination temperatures: (a) 450°C, (b) 550°C, (c) 650°C, (d) 750°C, (e) 850°C and (f) 950°C

Fig. 5 depicts the HRTEM images of TiO$_2$ sample annealed 650°C. As shown in Fig. 5, a mixed structure of TiO$_2$ nanotube and nanoparticle is observed. The diameter of the smooth nanotube ranges from 50 nm to 80 nm and the average particle size is near 60 nm.
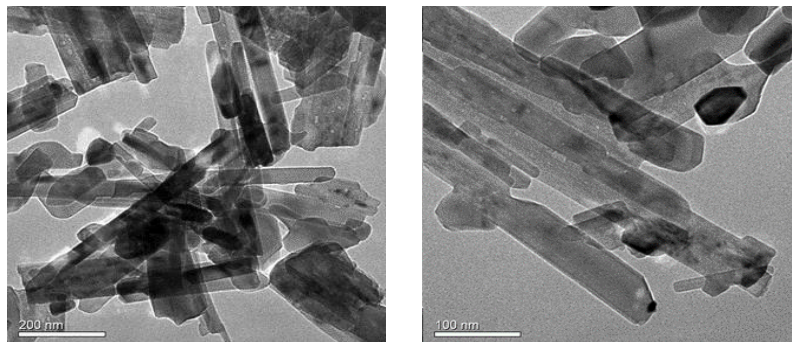

Fig. 5. HRTEM images of TiO$_2$ nanotubes annealed at 650°C.

The photocatalytic performance of TiO$_2$ nanotubes was analyzed by degradation of methylene blue aqueous solution. Fig. 6 shows the change of MB concentration with the irradiation time in the presence of various photocatalysts. It is found that the absorbance of MB dye solution decreases gradually with increasing irradiation time, indicating the MB solution has been removing.
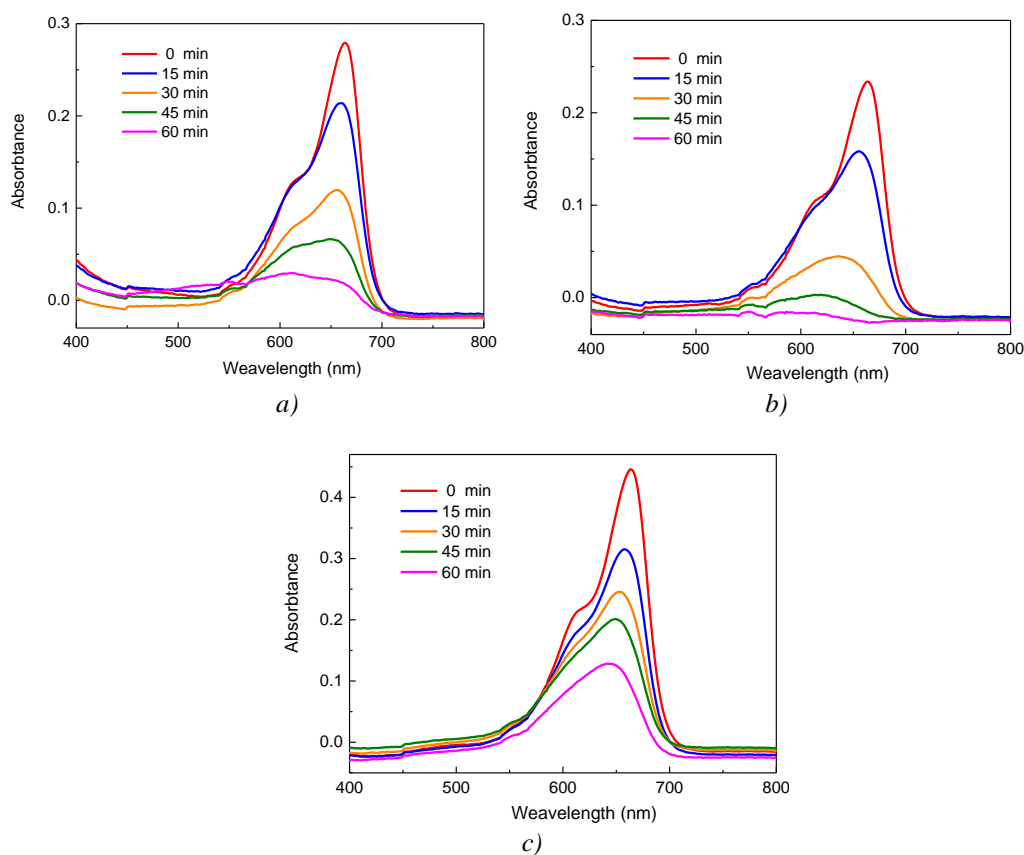

Fig. 6. UV-Vis absorption spectra of MB dye solution with different photocatalysts:
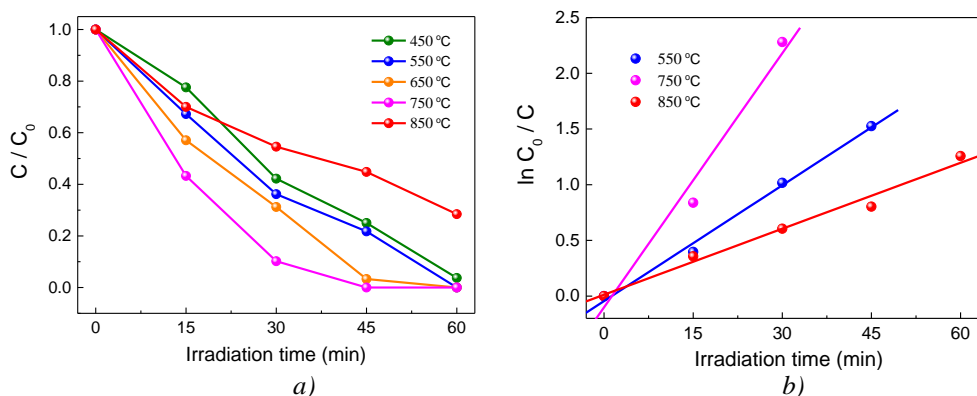*(a) TNT-550, (b) TNT-750, (c) TNT-850.*

Fig. 7. (a) Photocatalytic degradation behaviors of MB by TNTs calcined at different temperatures and (b) kinetic fit for the degradation of MB.

The photocatalytic activity of TNT samples is compared in Figure 7. As shown in Figure 7 (a), after reaction for 1 hour the photocatalytic degradation efficiency of MB is 96.3% and 71.6% for TNT-450 and TNT-850, respectively. For other samples TNT-650 and TNT-750, the photocatalytic degradation efficiency is very close to 100% only after irradiation for 45 minutes, which indicates TiO_2 nanotubes synthesized in this work demonstrate excellent photocatalytic activity. The kinetics curves of MB degradation rate are shown in Figure 7 (b), which follow the first-order Langmuir-Hinshelwood rate equation. It can be seen that the calcination temperature of TiO_2 nanotubes has a significant influence on the photocatalytic activity. As the calcination temperature below 750°C, the photocatalytic efficiency of MB increases with the increasing temperature due to the enhancement of the crystallinity of TiO_2. Though the nanotubular structure has begun to destroy at 650°C, the anatase phase and some remaining nanotubes also promote the degradation of MB. As the sample annealed at 750°C, the crystallinity is increased continuously and remains anatase phase. Furthermore, the nanorod structure could provide efficient route for charge transfer and then reduce the combination of photogenerated electron-hole pairs, which are conductive to improving degradation efficiency. Therefore, TiO_2 sample annealed at 750°C displays the highest photocatalytic activity. At higher calcination temperature than 750°C, rutile phase appears and the nanotubular structure has transformed to TiO_2 particles with large sizes and small surface area, leading to the decrease of degradation rate.

4. Conclusion

Using commercial P25 as raw material, one-dimensional TiO_2 nanotubes were prepared by hydrothermal method with different hydrothermal times and annealing temperatures. The formation process of nanotube structure was discussed via the morphology change in different hydrothermal durations. The annealing temperature significantly affects the crystalline structure, morphology and photocatalytic activity of TiO_2 nanotubes. At lower temperature (450 -550°C), TiO_2 exists in the form of TiO_2 (B) phase and remains the nanotubular structure. With further increase in calcination temperature, the crystallinity of TiO_2 is improved while the tubular structure has collapsed. At a higher temperature of 850°C, a mixed structure of anatase and rutile phase can be observed and TiO_2 nanotubes have completely transformed to TiO_2 particles. TiO_2 annealed at 750°C exhibits the highest photocatalytic activity due to the excellent crystallization of anatase phase and nanorod structure.

Acknowledgements

References

[1] Y. Sun, E. D. Liu, L. Zhu, Y. Wen, Q. W. Tan, W. Feng, Digest Journal of Nanomaterials and Biostructures **14** (2), 463 (2019).

[2] S. A. Hamdan, I. M. IbrahiM, I. M. Ali, Digest Journal of Nanomaterials and Biostructures **15** (4), 1001 (2020).

[3] M. A. K. L. Dissanayake, T. Liyanage, T. Jaseetharan, G. K. R. Senadeera, B. S. Dassanayake, Electrochimica Acta **347**, 136311 (2020).

[4] L. Wu, J. Zheng, L. Wang, X. Xiong, Y. Shao, G. Wang, J. Wang, S. Zhong, M. Wu, Angewandte Chemie International Edition **58**(3), 811 (2019).

[5] F. Jiang, S. Zheng, L. An, H. Chen, Applied Surface Science **258**(18), 7188 (2012).

[6] Y. Sun, Q. Zhao, G. X. Wang, K.P. Yan, IJournal of Alloys and Compounds **711**, 514 (2017).

[7] G. Zhang, H. Miao, X. Hu, J. Mu, X. Liu, T. Han, J. Fan, E. Liu, Y. Yin, J. Wan, Applied Surface Science **391**, 345 (2017).

[8] L. K. Tan, M. K. Kumar, W. W. An, H. Gao, Transparent, ACS Applied Materials & Interfaces **2**(2), 498 (2010).

[9] D. Lee, S. Lee, K.Y. Rhee, S. Park, Current Applied Physics **14**(3), 415 (2014).

[10] F. Zuo, K. Bozhilov, R.J. Dillon, L. Wang, P. Smith, X. Zhao, C. Bardeen, P. Feng, Angewandte Chemie International Edition **51**(25), 6223 (2012).

[11] Q. Luo, Q. Cai, X. Li, X. Chen, Journal of Alloys and Compounds **597**, 101 (2014).

[12] Y. Sun, Y. Gao, B. Zhao, S. Xu, C. Luo, Q. Zhao, Materials Research Express **7**(8), 85010 (2020).

[13] V. V. Burungale, V. V. Satale, A. J. More, K. K. K. Sharma, A. S. Kamble, J. H. Kim, P. S. Patil, Journal of Colloid and Interface Science **470**, 108 (2016).

[14] Y. Xu, M. Zhang, M. Zhang, J. Lv, X. Jiang, G. He, X. Song, Z. Sun, Applied Surface Science **315**, 299 (2014).

[15] M. Liu, H. Li, Y. Zeng, T. Huang, Applied Surface Science **274**, 117 (2013).

[16] J. Yu, J. Low, W. Xiao, P. Zhou, M. Jaroniec, Journal of the American Chemical Society **136**(25), 8839 (2014).

[17] Y. Sun, E. D. Liu, L. Zhu, Y. Wen, Q. W. Tan, W. Feng, Digest Journal of Nanomaterials and Biostructures **14**(2), 463 (2019).

[18] H. Yin, G. Ding, B. Gao, F. Huang, X. Xie, M. Jiang, Materials Research Bulletin **47**(11), 3124   12).

[19] S. H. Cho, G. Gyawali, R. Adhikari, T. H. Kim, S. W. Lee, Materials Chemistry and Physics **145**(3), 297 (2014).

[20] C. Guo, J. Xu, Y. He, Y. Zhang, Y. Wang, Applied Surface Science **257**(8), 3798 (2011).

[21] Q. Li, R. Liu, B. Zou, T. Cui, B. Liu, Physica B: Condensed Matter **445**, 42 (2014).

[22] D. Wu, J. Liu, X. Zhao, A. Li, Y. Chen, N. Ming, Chemistry of Materials **18**(2), 547 (2006).

[23] C. L. Wong, Y. N. Tan, A. R. Mohamed, Journal of Environmental Management **92**(7), 1669   11).

[24] W. Zhou, L. Gai, P. Hu, J. Cui, X. Liu, D. Wang, G. Li, H. Jiang, D. Liu, H. Liu, J. Wang, Crystengcomm **13**(22), 6643 (2011).

[25] C. Ai, P. Xie, X. Zhang, X. Zheng, J. Li, A. Kafizas, S. Lin, ACS Sustainable Chemistry & Engineering **7**(5), 5274 (2019).

[26] S. Shen, X. Wang, T. Chen, Z. Feng, C. Li, The Journal of Physical Chemistry C **118**(24), 12661 (2014).